

Theory of the valley-density wave and hidden order in iron pnictides

Jian Kang and Zlatko Tešanović

Institute for Quantum Matter and Department of Physics & Astronomy, The Johns Hopkins University, Baltimore, Maryland 21218, USA
(Received 20 November 2010; revised manuscript received 22 December 2010; published 31 January 2011)

In the limit of perfect nesting, the physics of iron pnictides is governed by the density wave formation at the zone-edge vector \mathbf{M} . At high energies, various spin- (SDW), charge-, and orbital/pocket- (PDW) density waves, and their linear combinations, all appear equally likely, unified within the unitary order parameter of $U(4) \times U(4)$ symmetry. Nesting imperfections and low-energy interactions reduce this symmetry to that of real materials. Nevertheless, the generic ground state preserves a distinct signature of its highly symmetric origins: A SDW along one axis of the iron lattice is predicted to *coexist* with a perpendicular PDW, accompanied by weak charge currents. This “hidden” order induces the structural transition in our theory, naturally insures $T_s \geq T_N$, and leads to orbital ferromagnetism and other observable consequences.

DOI: [10.1103/PhysRevB.83.020505](https://doi.org/10.1103/PhysRevB.83.020505)

PACS number(s): 74.70.Xa, 75.30.Fv, 75.25.Dk

The discovery of high-temperature superconductivity (HTS) in iron pnictides^{1,2} has sparked intense research.³ Like the cuprates, the pnictides are layered systems and exhibit antiferromagnetism (AF) at zero doping ($x = 0$), followed by HTS beyond some finite x .^{3,4} Magnetic order in parent compounds consists of an AF spin chain along the wave vector $(\pi, 0)$ or $(0, \pi)$ in the *unfolded* Brillouin zone (UBZ) and an FM spin chain along the perpendicular direction.⁵ The dynamical origin of this AF state is hotly debated: Within the itinerant electron model, the magnetic transition is ascribed to the SDW instability, enhanced by the near-nesting among electron and hole pockets of the Fermi surface (FS).^{6–9} To ensure “striped” spin order, only one electron pocket is involved in SDW, and the spin-wave anisotropy arises from the electron pockets’ finite ellipticity.^{10,11} In contrast, within the localized Heisenberg-type model^{12,13} various frustrated couplings J_{1a} , J_{1b} , J_2 between neighboring spins conspire to produce the observed magnetic order and the magnon anisotropy.^{14,15}

In addition, the tetrahedral-to-orthorhombic structural transformation is observed, accompanied by the AF transition.^{16,17} The AF-ordered moment is linearly proportional to orthorhombicity on change in x , and both transitions disappear for $x > x_c$.¹⁸ Magnetoelastic coupling was suggested as being responsible for the close relation between two transitions.¹⁹ In this approach, the structural transition is driven by magnetic interactions.²⁰ However, in the 1111 compounds, the structural transition temperature T_s is consistently above the AF one, T_N , at any x .⁵ Furthermore, the in-plane resistivity anisotropy develops well above T_N in the presence of uniaxial pressure, and hints at the appearance of a form of order near T_s .²¹ One possible explanation for $T_s > T_N$ is that magnetic fluctuations are much stronger than those associated with structural order.

In this Rapid Communication, we advance another physical picture to account for this evident close relation between the structural and magnetic transitions: the two are just different faucets of one and the same type of ordering of much higher, $U(4) \times U(4)$ symmetry. This high symmetry characterizes the dynamics of pnictides within the *high-energy* regime, extending from the energies of order of the bandwidth D down to those set by $T_s \sim T_N$. This regime is governed by “perfect” nesting and the ensuing tendency toward formation of a valley-density wave (VDW) at the nesting

vector \mathbf{Q} , with all of its different reincarnations—various spin-, charge-, and orbital/pocket-density waves (SDW, CDW, PDW, respectively), as well as their mutually orthogonal linear combinations—unified within a unitary $U(4) \times U(4)$ order parameter.²² At yet lower energies, however, as the $U(4) \times U(4)$ symmetry-breaking interactions and the deviations from perfect nesting come into play, the symmetry is reduced down to that of real materials. Nevertheless, provided there is a significant segregation of scales in the effective Hamiltonian of iron pnictides between the high-energy $U(4) \times U(4)$ -symmetric and the low-energy symmetry-breaking terms, the ground state and its excitations bear a distinct signature of their highly symmetric origin.

Our picture is based on the itinerant model and relies on the hierarchy of energy scales that separate the “flavor”-conserving from the “flavor”-changing interactions of quasiparticles on the FS, composed of two hole (h_1, h_2) and two electron (e_1, e_2) pockets (or valleys) (Fig. 1). This hierarchy is further assisted by the differences in area and shape of different pockets being much smaller than their common overall features; hence the $U(4)_e \times U(4)_h$ symmetry. Such hierarchy, quantified in Ref. [22], does not reflect a deep underlying principle; rather, it is an accident of the particular semimetallic character of pnictides and a screened Coulomb repulsion.²³ But be that as it may, the hierarchy is well obeyed in all parent compounds and we use it as an organizing framework to derive the following results: (i) The ground state of parent pnictides is the *combination* of a SDW along the wave vector $(\pi, 0)$ or $(0, \pi)$ in the UBZ and a spin-singlet density wave (DW) along the perpendicular direction; (ii) the spin-singlet DW is predominantly a PDW, with a tiny admixture of a CDW, and is imaginary, i.e., it represents a modulated pattern of weak currents on interiron bonds. This PDW is difficult to detect and is dubbed the “hidden” order; (iii) the imaginary PDW at $\mathbf{Q} = (\pi, 0)$ [or $(0, \pi)$] induces *real* CDW at $2\mathbf{Q} = (0, 0)$, differing from the CDW similarly generated by the SDW. The resulting broken orbital symmetry between e_x and e_y pockets (Fig. 1) drives the observed tetragonal-to-orthorhombic transition; and (iv) the predicted electronic structure of the ground state has numerous observable consequences, some of which we explore. Our results are generic for the 1111 and 122 materials, and—with

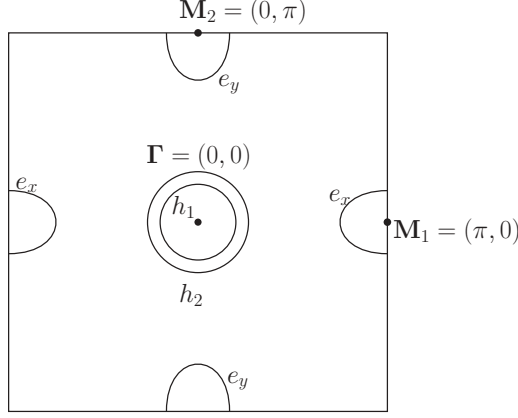


FIG. 1. Fermi pockets in the UBZ of iron pnictides. Two hole pockets h_1 and h_2 are centered at the $\Gamma = (0,0)$ point. The electron pockets e_x and e_y are centered at the nesting vectors $\mathbf{M}_1 = (\pi,0)$ and $\mathbf{M}_2 = (0,\pi)$, respectively. The h_1 , e_x , and e_y pockets are assumed to be perfectly nested to the leading order, while h_2 is larger than these three; this difference, however, is small compared to the overall bandwidth D , as is the finite but small ellipticity of e_x and e_y pockets.^{7,10}

details changing from one compound to another—the overall physical picture should be universally applicable.

First, we set up the problem as follows: the band structure can be described by the five $3d\text{Fe}$ and three $p\text{Pn}$ orbitals tight-binding model,⁷ resulting in the FS of Fig. 1. Our point of departure is the Hamiltonian $H = H_0 + H_W$:

$$H_0 = \sum_{\mathbf{k},\sigma,\alpha} \epsilon_{\mathbf{k}}^{\alpha} h_{\mathbf{k}\sigma}^{(\alpha)\dagger} h_{\mathbf{k}\sigma}^{(\alpha)} + \sum_{\mathbf{k},\sigma,\beta} \epsilon_{\mathbf{k}}^{\beta} e_{\mathbf{k}\sigma}^{(\beta)\dagger} e_{\mathbf{k}\sigma}^{(\beta)}$$

$$H_W = W \sum_{\mathbf{q}} \hat{n}_{\mathbf{q}}^e \hat{n}_{-\mathbf{q}}^h, \quad (1)$$

where σ, α , and β are the spin, hole (h), and (e) pocket indices, respectively (Fig. 1; $\beta = x, y$ for e bands, $\alpha = 1, 2$ for h bands) and $\hat{n}_{\mathbf{q}}^e$ and $\hat{n}_{\mathbf{q}}^h$ are the density operators within the e and h pockets.²²

H [Eq. (1)] describes the high-energy physics of pnictides. It contains only the density-density, flavor-conserving interactions between different pockets, $W \lesssim D$.²⁴ In contrast, the flavor-changing interactions and the variations among W s in different pockets are all $\ll D$, as long as the Hund coupling $J_H \ll U_d$, the Hubbard repulsion on d orbitals.^{7,22} Furthermore, we also initially assume perfect nesting, i.e., $\epsilon_{\mathbf{k}}^1 = \epsilon_{\mathbf{k}}^2 = -\epsilon_{\mathbf{k}+\mathbf{M}_1}^x = -\epsilon_{\mathbf{k}+\mathbf{M}_2}^y = \epsilon_{\mathbf{k}}$, since the differences among h and e bands are also $\ll D$.

H [Eq. (1)] has a large $U(4)_e \times U(4)_h$ symmetry, made manifest by introducing annihilation operators c_{μ} and d_{ν} to represent h and e pockets, respectively, with $\mu, \nu = 1, \dots, 4$ labeling both spin and band indices:

$$\mu, \nu = \begin{cases} 1 & h_{1\uparrow} \text{ or } e_{x\uparrow}; & 2 & h_{1\downarrow} \text{ or } e_{x\downarrow} \\ 3 & h_{2\uparrow} \text{ or } e_{y\uparrow}; & 4 & h_{2\downarrow} \text{ or } e_{y\downarrow} \end{cases}.$$

$$H_0 = \sum_{\mathbf{k}, \mu} \epsilon_{\mathbf{k}} (c_{\mu}^{\dagger} c_{\mu} - d_{\mu}^{\dagger} d_{\mu})$$

$$H_W = W \sum_{\mathbf{q}, \mu, \nu} c_{\mu\mathbf{k}+\mathbf{q}}^{\dagger} c_{\mu\mathbf{k}} d_{\nu\mathbf{k}'}^{\dagger} d_{\nu\mathbf{k}'+\mathbf{q}}.$$

The interaction H_W drives a VDW formation at the nesting vectors \mathbf{M}_1 and \mathbf{M}_2 (Fig. 1). The order parameter is a 4×4 matrix $\Delta_{\mu\nu}$ whose 16 complex elements describe various SDWs, CDWs, PDWs, and their linear combinations that gap the FS below some temperature T_V :

$$\exp\left(-W \sum c_{\mu}^{\dagger} c_{\mu} d_{\nu}^{\dagger} d_{\nu}\right)$$

$$\Leftrightarrow \int \mathcal{D}\Delta \exp\left\{-\sum_{\mu\nu} \left[\frac{1}{W} |\Delta_{\mu\nu}|^2 - \Delta_{\mu\nu}^* c_{\mu}^{\dagger} d_{\nu} + \text{H.c.}\right]\right\}.$$

Integrating out the fermions yields an effective action \mathcal{S}_{Δ} for bosonic fields $\Delta_{\mu\nu}$. $\mathcal{S}_{\Delta}[\Delta_{\mu\nu}]$ has the $U(4)_e \times U(4)_h$ symmetry, spontaneously broken at T_V . Near T_V , a Ginzburg-Landau (GL) expansion in $\Delta_{\mu\nu}$ gives²⁵:

$$T\mathcal{S}_{\Delta} \rightarrow F = \alpha \text{Tr}(\Delta^{\dagger} \Delta) + \frac{1}{2} \beta \text{Tr}(\Delta^{\dagger} \Delta \Delta^{\dagger} \Delta), \quad (2)$$

$$\alpha = \frac{1}{W} - \frac{T}{N} \sum_{k,n} \frac{1}{\omega_n^2 + \epsilon_k^2} \approx \frac{1}{W} - N(0) \ln\left(\frac{D}{T}\right), \quad (3)$$

$$\beta = \frac{T}{2N} \sum_{k,n} \left(\frac{1}{\omega_n^2 + \epsilon_k^2}\right)^2 = \frac{7}{16\pi^2} \frac{N(0)}{T^2} \zeta(3),$$

where $N(0)$ is the density of states of a Fermi pocket and $\{\omega_n\}$ are Matsubara frequencies. For $T < T_V$, $\alpha < 0$ and F has a nontrivial minimum for $\Delta^{\dagger} \Delta = \Delta_0^2 = -\alpha/\beta$. The solution is $\Delta = \Delta_0 \mathcal{U}$, where \mathcal{U} is a 4×4 unitary matrix. At this stage, the four complex four-vectors comprising \mathcal{U} describe a plethora of SDWs, CDWs, PDWs, etc., and all their mutually orthogonal linear combinations.

Now, we are ready to confront the real iron pnictides. We turn on all low-energy ($\ll D \sim W$) features ignored in Eq. (1)—differences among W s, flavor-changing vertices, nesting imperfections, and the like²⁴—and proceed to systematically decode their effect on the $U(4)_e \times U(4)_h$ symmetric theory.²⁶ The most important among these is the interband vertex G_2 , which generates the s^{\pm} superconductivity as the nesting subsides^{6,7}:

$$[G_2^{eh_1} c_1^{\dagger} c_2^{\dagger} (d_2 d_1 + d_4 d_3) + G_2^{eh_2} c_3^{\dagger} c_4^{\dagger} (d_2 d_1 + d_4 d_3)] + \text{H.c.},$$

where $G_2^{eh_{\alpha}} = G_2^{e_x h_{\alpha}} = G_2^{e_y h_{\alpha}}$.²⁷ The leading-order correction ΔF^{G_2} [Fig. 2(a)] to the free energy F (2) is

$$\sim \Pi(0)^2 \{G_2^{eh_1} (\Delta_{11} \Delta_{22} + \Delta_{13} \Delta_{24} - \Delta_{12} \Delta_{21} - \Delta_{14} \Delta_{23})$$

$$+ G_2^{eh_2} (\Delta_{31} \Delta_{42} + \Delta_{33} \Delta_{44} - \Delta_{32} \Delta_{41} - \Delta_{34} \Delta_{43}) + \text{H.c.}\},$$

$\Pi(0) \approx N(0) \ln(\frac{D}{T})$.²⁷ The Cauchy inequality mandates $\Delta F^{G_2} \geq -\Pi(0)^2 \Delta_0^2 (|G_2^{eh_1}| + |G_2^{eh_2}|)$. The equality holds when (a) for $G_2^{eh_1} > 0$, $\Delta_{22} = -\Delta_{11}^*$, $\Delta_{21} = \Delta_{12}^*$, $\Delta_{24} = -\Delta_{13}^*$, $\Delta_{23} = \Delta_{14}^*$. The VDW involving the h_1 pocket is then the mixture of real SDW and imaginary spin-singlet DW; (b) for $G_2^{eh_1} < 0$, the VDW involving h_1 pocket is similarly the mixture of imaginary SDW and real spin-singlet DW. The same holds for the h_2 pocket.

Consequently, G_2 fixes the phases of different DWs. One expects that both $G_2^{eh_1}, G_2^{eh_2} > 0$, as the prerequisite for high T_c s^{\pm} superconductivity. Hence, the ground state of parent compounds must be composed of either real SDW(s) or imaginary spin-singlet DW(s); the latter is a general combination

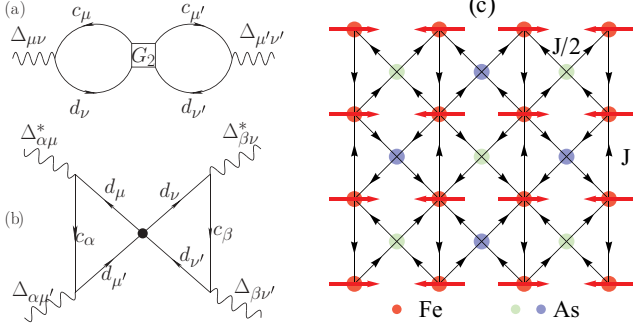


FIG. 2. (Color) The leading-order corrections to F due to (a) e - h and (b) e - e interactions. (c) The ground state of parent iron pnictides. The red and black arrows depict iron spins and the $[\pm\mathcal{J}, \pm\frac{1}{2}\mathcal{J}]$ current pattern, respectively. The ground state combines two orders: SDW along $(\pi, 0)$ and the modulated current DW at the wave vector $(0, \pi)$, i.e., the “hidden” order.

of PDW and CDW, in the nomenclature of Ref. [28]. The real DWs are $\propto \cos(\mathbf{M} \cdot \mathbf{r})$, with peaks and troughs on the iron sites [Fig. 2(c)]. In contrast, the imaginary spin-singlet DW breaks time-reversal and lattice translation symmetries along \mathbf{M} , leading to charge or orbital current DW on iron bonds.

But which one is it, a spin-triplet (SDW) or spin-singlet (PDW/CDW) density wave? We must consider next the flavor-changing p- h analog of G_2 , G_1 : $\sum_{\alpha, \beta=1}^2 G_1^{\alpha\beta} h_{\alpha\sigma}^\dagger (e_{x\sigma} e_{x\sigma'}^\dagger + e_{y\sigma} e_{y\sigma'}^\dagger) h_{\beta\sigma'}$. G_1 ($< G_2^{22}$) generates ΔF^{G_1} from a diagram similar to Fig. 2(a):

$$\begin{aligned} \Delta F^{G_1} = & \Pi(0)^2 \{ G_1^{11} (|\Delta_{11} + \Delta_{22}|^2 + |\Delta_{13} + \Delta_{24}|^2) \\ & + G_1^{22} (|\Delta_{31} + \Delta_{42}|^2 + |\Delta_{33} + \Delta_{44}|^2) \\ & + [G_1^{12} (\Delta_{11}^* + \Delta_{22}^*) (\Delta_{31} + \Delta_{42}) + \text{H.c.}] \\ & + [G_1^{12} (\Delta_{13}^* + \Delta_{24}^*) (\Delta_{33} + \Delta_{44}) + \text{H.c.}] \}. \end{aligned} \quad (4)$$

Here, it is useful to introduce 2×2 G_1 matrix

$$G_1 = \begin{pmatrix} G_1^{11} & \text{Re} G_1^{12} \\ \text{Re} G_1^{21} & G_1^{22} \end{pmatrix}.$$

Since the phases of DWs are fixed by G_2 , only the real parts of $G_1^{\alpha\beta}$ contribute to F . Hence, G_1 is real and symmetric and has two real eigenvalues λ_1, λ_2 , with associated real eigenvectors v_1 and v_2 . From (4), $\Delta F^{G_1} = 0$ for SDW and is minimized for the state composed of (a) if $\lambda_1, \lambda_2 > 0$, two real SDWs; (b) if $\lambda_1, \lambda_2 < 0$, two imaginary spin-singlet DWs, with $\Delta F^{G_1} = (\lambda_1 + \lambda_2) \Pi(0)^2 \Delta_0^2 < 0$; and (c) if $\lambda_1 < 0$ and $\lambda_2 > 0$, one real SDW and one imaginary spin-singlet DW, with $\Delta F^{G_1} = \lambda_1 \Pi(0)^2 \Delta_0^2 < 0$. Experimentally, there is only a single SDW at $(\pi, 0)$. This implies option (c): with majority of G_1 s rather small,²² this is to be expected, once we include the (weak) electron-phonon coupling and large polarizability of p orbitals.^{3,4} In this case, the leading-order contribution of ΔF^{G_2} and ΔF^{G_1} to F is

$$F \approx \alpha (\Delta_{\text{SDW}}^2 + \Delta_{\text{SSDW}}^2) + \lambda_1 \Pi(0)^2 \Delta_{\text{SSDW}}^2.$$

Δ_{SDW} and $i \Delta_{\text{SSDW}}$ describe the SDW and the imaginary spin-singlet DW, respectively, while

$$\begin{aligned} \alpha(T_{\text{SDW}}) = 0 \quad \alpha(T_{\text{SSDW}}) + \lambda_1 \Pi(0)^2 &= 0, \\ \frac{T_{\text{SSDW}} - T_{\text{SDW}}}{T_{\text{SDW}}} &\approx -\frac{\lambda_1/W}{N(0)W} > 0, \end{aligned}$$

set the corresponding transition temperatures. As long as $|\lambda_1| \ll W$,²² $T_{\text{SSDW}} \gtrsim T_{\text{SDW}}$ and $\Delta_{\text{SSDW}} \gtrsim \Delta_{\text{SDW}}$.

Consider now $v_1 = (a, b)$, the (real) eigenvector associated with $\lambda_1 < 0$. ΔF^{G_1} is minimized by

$$\Delta(\theta) = \Delta_0 \begin{pmatrix} ia\mathbb{1} & -b\sigma_n \\ ib\mathbb{1} & a\sigma_n \end{pmatrix} \times \begin{pmatrix} \cos\theta\mathbb{1} & -\sin\theta\mathbb{1} \\ \sin\theta\mathbb{1} & \cos\theta\mathbb{1} \end{pmatrix}, \quad (5)$$

where $\sigma_n = \vec{\sigma} \cdot \hat{n}$, \hat{n} is an arbitrary unit vector reflecting the SU(2) spin symmetry of our theory, and θ is an arbitrary angle, signaling an additional degeneracy in the Hamiltonian. The second matrix in (5) is a rotation by θ which mixes e_x and e_y pockets:

$$e_1 = \cos\theta e_x - \sin\theta e_y, e_2 = \cos\theta e_y + \sin\theta e_x. \quad (6)$$

In the state described by (5), e_1 and e_2 couple to $h_n = ah_1 + bh_2$ and $h_p = ah_2 - bh_1$, respectively, to form two DWs. Finally, this remaining θ degeneracy is lifted by the density-density repulsion between e_x and e_y pockets:

$$W_k^e e_{x\sigma}^\dagger e_{x\sigma'} e_{y\sigma'}^\dagger e_{y\sigma} \rightarrow W_k^e (d_1^\dagger d_1 + d_2^\dagger d_2)(d_3^\dagger d_3 + d_4^\dagger d_4),$$

with $W_k^e > 0$. The leading-order contribution to F , ΔF^{W_k} , follows from Fig. 2(b) and contains two fermion loops, each with three legs. Were the nesting perfect, the loop integral would be independent of leg indices, and, on summation over hole indices, the contribution of each loop would be $\propto \Delta^\dagger \Delta$ but still independent of θ .

In real pnictides, however, the outer pocket h_2 deviates significantly from h_1 and perfect nesting (Fig. 1).^{3,7,29} To account for this, we set $\epsilon_{\mathbf{k}}^{h_2} = \epsilon_{\mathbf{k}}^{h_1} + \eta$, $\eta \ll W \lesssim D$. At the leading order in η , the θ -dependent term of each fermion loop in Fig. 2(b) is now finite and contributes

$$\begin{aligned} \frac{1}{N} \sum_{\omega, \mathbf{k}} \left(\frac{1}{i\omega + \epsilon} \right)^2 \frac{\eta}{(i\omega - \epsilon)^2} \\ = 2\beta\eta \rightarrow \Delta F^{W_k} \sim 2W_k^e (2\beta\eta)^2 \Delta_0^2 [(a \cos\theta)^2 + (b \sin\theta)^2] \\ \times [(a \sin\theta)^2 + (b \cos\theta)^2] \alpha(ab)^2 + (b^2 - a^2)^2 \cos^2\theta \sin^2\theta. \end{aligned}$$

Since generally $|a| \neq |b|$, ΔF^{W_k} is minimized for $\theta = 0$ or $\pi/2$. Thus, the preferred ground state combines a real SDW in one direction and an imaginary spin-singlet DW along the perpendicular direction. The nature of this imaginary spin-singlet DW depends on the form of v_1 .³⁰ If $a \approx -b$, the spin-singlet DW is predominantly a PDW, translating into a purely orbital current pattern. However, unless $a = -b$, there is also an accompanying charge current DW, depicted in Fig. 2(c). This current DW can be weak for generic $a \sim -b$ but should be observable and is the main prediction of this Rapid Communication. Since the charge current DW

interacts with the underlying lattice more strongly than the pure PDW, it favors an additional modulated structural pattern along $(0, \pi)$, on top of the one tied to the SDW along $(\pi, 0)$. The apparent absence of such pattern in pnictides suggests that indeed $a \approx -b$ and the PDW dominates the imaginary spin-singlet DW.

With two DWs present at $\mathbf{Q} = \mathbf{M}_1$ and \mathbf{M}_2 , a real CDW at $2\mathbf{Q} = (0, 0)$ is induced as a next harmonic.³¹ First, this is illustrated within a two-band model, with one h and one e pocket. In the mean-field approximation:

$$H_{\text{MF}} = \delta\Sigma(h_{\mathbf{k}\sigma}^\dagger h_{\mathbf{k}\sigma} - e_{\mathbf{k}\sigma}^\dagger e_{\mathbf{k}\sigma}); \quad H_U = U(\hat{n}_h^2 + \hat{n}_e^2),$$

$$F \leq F_{\text{MF}} + \langle H_U - H_{\text{MF}} \rangle_{\text{MF}}. \quad (7)$$

U is the intrapocket repulsion and $\delta\Sigma$ is the relative shift of h and e self-energies. Here we assume the e pocket dispersion is $\epsilon_{\mathbf{k}} = k^2/2m - \epsilon_0$. For $\delta\Sigma \ll \Delta_0$,

$$F_{\text{MF}} = \alpha(\delta\Sigma)\text{Tr}(\Delta^\dagger \Delta) + O(\Delta^4),$$

$$\alpha(\delta\Sigma) = \frac{1}{W} - \frac{1}{\beta} \sum_n \int_{-\epsilon_0 - \delta\Sigma}^D d\epsilon \frac{N(0)}{\epsilon^2 + \omega_n^2} \approx \alpha(0) - \delta\Sigma \frac{N(0)}{2\epsilon_0},$$

$$\langle \delta n_e \rangle = -\langle \delta n_h \rangle \approx N(0)\delta\Sigma,$$

$$\langle H_U - H_{\text{MF}} \rangle_{\text{MF}} \approx 2N(0)(\delta\Sigma)^2 [1 + N(0)U].$$

The right-hand side of (7) is minimized when $\delta\Sigma = \Delta_0^2 / \{8\epsilon_0[1 + N(0)U]\}$, and hence, $\langle \delta n_e \rangle = -\langle \delta n_h \rangle = \frac{N(0)\Delta_0^3}{8\epsilon_0[1 + N(0)U]}$.

In a realistic four-band model, with the induced CDWs at $2\mathbf{Q}$, a lengthy but straightforward algebra yields²⁶

$$\langle \delta n_{e_x} \rangle = -\langle \delta n_{h_p} \rangle = \frac{N(0)}{8\epsilon_0[1 + N(0)U]} \Delta_{\text{SDW}}^2, \quad (8)$$

$$\langle \delta n_{e_y} \rangle = -\langle \delta n_{h_n} \rangle = \frac{N(0)}{8\epsilon_0[1 + N(0)U]} \Delta_{\text{PDW}}^2.$$

As shown earlier, $\Delta_{\text{SDW}} < \Delta_{\text{PDW}}$, and thus $\langle e_y^\dagger e_y \rangle > \langle e_x^\dagger e_x \rangle$ implying unequal occupancy and splitting of d_{xz} and d_{yz} orbitals. Consequently, the induced real CDW at $2\mathbf{Q} = (0, 0)$ is an orbital ferromagnet which breaks the C_4 symmetry while preserving the lattice translation symmetry and can be naturally identified as the source of the observed tetragonal-to-orthorhombic distortion. Since the CDW arises simultaneously with the modulated DWs, $T_s = T_{\text{PDW}} \geq T_N = T_{\text{SDW}}$. For $T \ll T_{\text{SDW}}$ and $0 < x \ll x_c$, Eqs. (8) also result in orthorhombicity $\propto \Delta_{\text{SDW}}(x)$, in agreement with.¹⁸ Additional support for this picture of structural deformation comes from the universal scaling of magnetization.³²

In summary, we have shown that the high-energy $U(4) \times U(4)$ symmetry in iron pnictides naturally leads to the prediction of a “hidden” orbital current DW order in parent compounds near the $\lambda_1 = 0$ quantum critical point and have explored some of the observable consequences.

We thank V. Cvetkovic for discussions and for sharing his insights with us. This work was supported in part by the Johns Hopkins–Princeton Institute for Quantum Matter, under Award No. DE-FG02-08ER46544 by the US Department of Energy, Office of Basic Energy Sciences, Division of Materials Sciences and Engineering.

¹Y. Kamihara *et al.*, *J. Am. Chem. Soc.* **130**, 3296 (2008).

²M. Rotter, M. Tegel, and D. Johrendt, *Phys. Rev. Lett.* **101**, 107006 (2008).

³J. Paglione and R. L. Greene, *Nat. Phys.* **6**, 645 (2010).

⁴I. I. Mazin *et al.*, *Phys. Rev. Lett.* **101**, 057003 (2008).

⁵C. de la Cruz *et al.*, *Nature (London)* **453**, 899 (2008).

⁶A. V. Chubukov, D. V. Efremov, and I. Eremin, *Phys. Rev. B* **78**, 134512 (2008).

⁷V. Cvetkovic and Z. Tesanovic, *Europhys. Lett.* **85**, 37002 (2009).

⁸F. Wang *et al.*, *Phys. Rev. Lett.* **102**, 047005 (2009).

⁹J. Dong *et al.*, *Europhys. Lett.* **83**, 27006 (2008).

¹⁰I. Eremin and A. V. Chubukov, *Phys. Rev. B* **81**, 024511 (2010).

¹¹J. Knolle *et al.*, *Phys. Rev. B* **81**, 140506(R) (2010).

¹²Q. Si and E. Abrahams, *Phys. Rev. Lett.* **101**, 076401 (2008).

¹³K. Seo, B. A. Bernevig, and J. Hu, *Phys. Rev. Lett.* **101**, 206404 (2008).

¹⁴J. Zhao *et al.*, *Nat. Phys.* **5**, 555 (2009).

¹⁵S. O. Diallo *et al.*, *Phys. Rev. Lett.* **102**, 187206 (2009).

¹⁶M. A. McGuire *et al.*, *Phys. Rev. B* **78**, 094517 (2008).

¹⁷S. D. Wilson *et al.*, *Phys. Rev. B* **79**, 184519 (2009).

¹⁸C. de la Cruz *et al.*, *Phys. Rev. Lett.* **104**, 017204 (2010).

¹⁹A. Cano *et al.*, *Phys. Rev. B* **82**, 020408 (2010).

²⁰V. Barzykin and L. P. Gor'kov, *Phys. Rev. B* **79**, 134510 (2009).

²¹J. H. Chu *et al.*, *Science* **329**, 824 (2010).

²²V. Cvetkovic and Z. Tesanovic, *Phys. Rev. B* **80**, 024512 (2009).

²³Unlike, say, the emergent low-energy $SO(6)$ symmetry of D. Podolsky *et al.*, *Europhys. Lett.* **88**, 17004 (2009).

²⁴The intraband repulsion is already implicitly included in (1) through renormalized bandwidths and other harmless Fermi-liquid renormalizations.

²⁵Note that the GL expansion is by no means necessary and is used only to make our presentation manageable.

²⁶For clarity, this is done to the leading order. The basic results, however, are robust and remain valid to all orders, as long as the energy hierarchy remains in place, as is evident from the text.

²⁷To streamline the text, we have suppressed the \mathbf{k} dependence and set the spin singlet and triplet contributions of G_2 to be equal, at the leading order. A laborious calculation, using G_2 's full momentum and orbital structure, leads to same conclusions; J. Kang (unpublished).

²⁸H. Zhai, F. Wang, and D.-H. Lee, *Phys. Rev. B* **80**, 064517 (2009).

²⁹D. H. Lu *et al.*, *Nature (London)* **455**, 81 (2008).

³⁰The variations in W s ($\ll W \lesssim D$) (1) enter here and modify the precise values of a and b , albeit only at the subleading, quadratic order. The same holds for η .

³¹J.-J. Su, Y. Dubi, P. Woelfle, and A. V. Balatsky (unpublished) and references therein.

³²S. D. Wilson, C. R. Rotundu, Z. Yamani, P. N. Valdivia, B. Freelon, E. Bourret-Courchesne, and R. J. Birgeneau, *Phys. Rev. B* **81**, 014501 (2010).